Magnetic anisotropy and slow magnetic relaxation processes of cobalt(II)-pseudohalide complexes

Journal:	*Dalton Transactions*
Manuscript ID	DT-ART-02-2019-000644.R1
Article Type:	Paper
Date Submitted by the Author:	04-Jun-2019
Complete List of Authors:	Cui, Hui-Hui; Nanjing University, State Key Laboratory of Coordination Chemistry Zhang, Yi-Quan; Nanjing Normal University, School of Physical Science and Technology Chen, Xue-tai; Nanjing University, State Key Laboratory of Coordination Chemistry Wang, Zhenxing; Huazhong University of Science and Technology, Wuhan National High Magnetic Field Center Xue, Zi-Ling; University of Tennessee, Department of Chemistry

Journal Name

ARTICLE

Magnetic anisotropy and slow magnetic relaxation processes of cobalt(II)-pseudohalide complexes

Received 00th January 20xx,
Accepted 00th January 20xx

DOI: 10.1039/x0xx00000x

www.rsc.org/

Hui-Hui Cui,[a] Yi-Quan Zhang,*[b] Xue-Tai Chen,[a,]* Zhenxing Wang,[c,]*and Zi-Ling Xue[d]

Three mononuclear six-coordinate Co(II)-pseudohalide complexes [Co(L)X_2] with two N-donor pseudohalido coligands occupying in the cis-positions (X = NCS^- (**1**), $NCSe^-$ (**2**) or $N(CN)_2^-$ (**3**)), and a five-coordinate complex [Co(L)(NCO)][$B(C_6H_5)_4$] (**4**) [L = macrocyclic ligand 1, 4, 7, 10-tetramethyl-1, 4, 7, 10-tetraazacyclododecane (12TMC)], have been prepared and structurally characterized. Easy-plane magnetic anisotropy for **1**-**3** and easy-axis anisotropy for **4** were revealed via the analyses of the direct-current magnetic data, high–frequency and –field EPR (HFEPR) spectra and ab initio theoretical calculations. They display slow magnetic relaxations under an external applied dc field. Typically, two slow relaxation processes were found in **1** and **2** while only one relaxation process occurs in **3** and **4**. The Raman-like mechanism is found to be dominant in the studied temperature range in **1**. For **2**-4, the Raman process is dominant in the low temperature region, while the Orbach mechanism dominates in the high temperature range.

Introduction

Single-molecule magnets (SMMs) display slow magnetic relaxation and magnetic hysteresis arising from the electronic structure at molecular level and have attracted much attention due to the forward-looking applications such as quantum computing,[1] spintronic devices,[2] and high density data storage.[3] Single ion magnets, which contain a unique paramagnetic center, form an important subclass of SMMs. The extensive research has been conducted to understand the origin and mechanism of slow magnetic relaxation and to improve the performance of single ion magnets, especially the lanthanide-based single molecule magnets.[4] Meanwhile, many transition-metal single ion magnets with various coordination numbers[5-18] have been reported since the discovery of the first 3d-ion mononuclear single ion magnets based on mononuclear trigonal pyramidal Fe(II) complex in 2010 by Long and co-workers.[8a]

The Co(II) ion has been frequently used to construct molecule-based magnets because of its strong magnetic anisotropy derived from the spin-orbital coupling. Moreover, Co(II) complexes have a high accessibility to model the magnetic behavior through tuning the coordination number, geometry and electronic structure. To date, a variety of different coordination geometries of Co(II)-based single ion magnets, including linear[11], trigonal,[12] tetrahedral,[13] square-pyramidal,[14] distorted octahedral[15] pentagonal bipyramid[16] and square antiprism,[17] have been designed to attain strong magnetic anisotropy. Besides the coordination geometry, the nature of donor atoms has also been used to tune the magnetic anisotropy. In this regard, several studies have showed that heavier donor atoms like S, Se, Te, P and As would give larger and negative anisotropy in metal complexes.[18] The changing of one or two terminal ligands such as halides could also modulate magnetic anisotropy and magnetic dynamics in several Co(II) complexes.[13e,f,14b] Only few studies are focused on the tuning of magnetic anisotropy by systematically changing the other terminal ligands such as the pseudohalides.[15d]

Recently, our group has reported two five-coordinate Co(II) complexes [Co(12-TMC)(CH_3CN)]$(X)_2$ (12-TMC = 1,4,7,10-tetramethyl-1,4,7,10-tetraazacyclododecane, X = BF_4^-, PF_6^-), which are the first examples of the coexistence of field induced slow magnetic relaxation and spin-crossover.[19] The coordination of tetradentate macrocyclic ligand 12-TMC would compel the Co(II) center out of the macrocyclic plane and leave one or two vacant sites accessible for further coordination. The metal coordination environment can thus be modified through simply using the different co-ligand to occupy the vacant coordinate sites. The co-ligands are expected to finely tune the magnetic anisotropy.

Herein we present the synthesis and magnetic properties of three mononuclear six-coordinate Co(II) complexes [Co(12TMC)X_2] with different pseudohalides, NCS^- (**1**), $NCSe^-$ (**2**) and $N(CN)_2^-$ (**3**), and one five-coordinate complex [Co(12TMC)(NCO)][$B(C_6H_5)_4$] (**4**). The easy-plane magnetic anisotropy has been confirmed for the six-coordinate complexes **1**-**3** by magnetometry and high–frequency and –field EPR (HFEPR) spectroscopy. In contrast, the easy-axis

---

[a] *State Key Laboratory of Coordination Chemistry, School of Chemistry and Chemical Engineering, Nanjing University, Nanjing 210023, China. E-mail: xtchen@nju.edu.cn.*
[b] *Jiangsu Key Laboratory for NSLSCS, School of Physical Science and Technology, Nanjing Normal University, Nanjing 210023, China*
[c] *Wuhan National High Magnetic Field Center, Huazhong University of Science and Technology, Wuhan 430074, China*
[d] *Department of Chemistry, University of Tennessee, Knoxville, Tennessee 37996, USA.*

†Electronic supplementary information (ESI) available: Figures of XRD patterns for 1-4; Table for the calculations by SHAPE; Table for the fitting data for the Cole-Cole plot; Additional figures for magnetic characterization and HFEPR data; Additional structural data in CIF format (CIF).See DOI: 10.1039/x0xx00000x

anisotropy was found for **4**. The ac susceptibility measurements demonstrate that they exhibit slow magnetic relaxation under an applied direct-current (dc) field. Remarkably, there are two relaxation processes observed in **1** and **2**. Details of the relaxation dynamics of magnetization are reported below.

Experimental

Materials and methods

All the solvents were dried and purified before use using conventional methods. The other chemicals employed were commercially available and used as received. 1,4,7,10-Tetramethyl-1,4,7,10-tetraazacyclododecane (12-TMC) was synthesized according to the literature procedure.[20] The synthetic experiments were carried out under N_2 atmosphere with standard Schlenk techniques. Elemental analyses of C, H and N were performed on an Elementar Vario ELIII elemental analyzer. Powder X-ray diffraction (PXRD) patterns were measured on a Bruker D8 ADVANCE X-ray powder diffractometer with a Cu Kα X-ray source (λ = 1.54056 Å). The phase purities of the complexes were confirmed with good agreement between the measured X-ray diffraction patterns and the simulated ones (Fig. S1-S4, ESI†). High-frequency and –field EPR (HFEPR) experiments were performed using a spectrometer constructed at the National High Magnetic Field Laboratory, USA.[21]

Synthesis of complexes 1-4

[Co(12-TMC)(NCS)$_2$]·0.5CH$_3$OH (1). Co(NCS)$_2$ (0.5 mmol, 0.095 g) and 12-TMC (0.5 mmol, 0.09 g) were dissolved in 15 mL of CH_3OH and stirred for 5 h at room temperature. A purple solution was formed and then filtered. Purple crystals of **1** were obtained after several days by the diffusion of diethyl ether into the filtrate, with a yield of 70% based on Co. Anal. Calc. for $C_{29}H_{60}Co_2N_{12}OS_4$: C, 41.52; H, 7.21; N, 20.03. Found: C, 41.58; H, 7.20; N, 20.10.

[Co(12-TMC)(NCSe)$_2$]·0.5CH$_3$CN (2). $CoCl_2$ (0.5 mmol, 0.065 g) and 12-TMC (0.5 mmol, 0.09 g) were dissolved in 15 mL of C_2H_5OH and stirred for 30 min at room temperature. KNCSe (1.0 mmol, 0.15 g) was added to the solution and stirred for another 5 h to give a purple precipitate. The precipitate was dissolved in acetonitrile and filtered to yield a purple solution. Purple crystals of **2** formed over several days by the diffusion of diethyl ether into the CH_3CN solution with a yield of 65% based on Co. Anal. Calc. for $C_{30}H_{59}Co_2N_{13}Se_4$: C, 34.79; H, 5.74; N, 17.58. Found: C, 34.75; H, 5.71; N, 17.60.

[Co(12-TMC)(N(CN)$_2$)$_2$] (3). **3** was obtained according to the same procedure as **2**, but using 12-TMC (1.0 mmol, 0.18 g) and NaN(CN)$_2$ (1.0 mmol, 0.089 g) instead of 12-TMC (0.5 mmol, 0.09 g) KNCSe (1.0 mmol, 0.15g). The red crystals of **3** were obtained in 70% yield based on Co. Anal. Calc. for $C_{16}H_{28}CoN_{10}$: C, 45.82; H, 6.73; N, 33.40. Found: C, 45.80; H, 6.71; N, 33.43.

[Co(12-TMC)(NCO)][B(C$_6$H$_5$)$_4$] (4). $CoCl_2$ (0.5 mmol, 0.065 g) and 12-TMC (1.0 mmol, 0.18 g) were dissolved in 15 mL of C_2H_5OH and stirred for 30 min at room temperature. KNCO (0.5 mmol, 0.04 g) and Na[B(C$_6$H$_5$)$_4$] (0.5 mmol, 0.17 g) was added to the solution and stirred for another 5 h. The resulting blue precipitate was collected and then dissolved in 15 mL acetonitrile. The blue crystals of **4** formed over several days by the diffusion of diethyl ether into the solution with a yield of 71% based on Co. Anal. Calc. for $C_{37}H_{48}BCoN_5O$: C, 68.52; H, 7.46; N, 10.80. Found: C, 68.49; H, 7.45; N, 10.81.

X-ray single-crystal structure determination

Single-crystal X-ray diffraction data were collected on a Bruker APEX DUO diffractometer at 155 K with a CCD area detector (Mo Kα radiation, λ = 0.71073 Å).[22] The APEX II program was employed to collect data and determine the unit-cell parameters. The collected data was integrated by SAINT and corrected for Lorentz and polarization effects.[23] Absorption corrections were applied using the multiscan program SADABS.[24] The molecular structures were determined via full-matrix least-squares procedure SHELXL (version 2014/7).[25] The hydrogen bonded to carbon were generated theoretically with isotropic thermal parameters riding on their parents. All non-hydrogen atoms were refined through full-matrix least-squares routine. A summary of the crystallographic data and refinement parameters are listed in Table S1.†

Magnetic measurements

Magnetic characterizations were carried out on a vibrating sample magnetometer (VSM) of Quantum Design MPMS SQUID-VSM system for ground microcrystalline powder of **1**-**4** restrained with eicosane within a polycarbonate plastic capsule in order to prevent solvent molecules from disappearance or any torquing caused by magnetic field. Direct-current (dc) magnetic data were collected in fields between 0 and 7 T at a temperature between 2 K and 300 K. Alternating-current (ac) susceptibility measurements were performed with an ac field of 0.2 mT at frequencies varying over the range of 1 to 999 Hz under different external fields. All experimental susceptibilities data were corrected for the diamagnetic contributions using Pascal's constants, included the sample holder as well as the diamagnetism of the sample.[26]

Results and discussion

Synthesis

Initially we employed the reactions between Co^{2+} and 12TMC to synthesize the six-coordinate [(12-TMC)CoX$_2$], with the different pseudohalides (NCS$^-$, NCSe$^-$, NCO and N(CN)$_2$$^-$). The six-coordinate complexes **1**-**3** were expectedly obtained with X = NCS$^-$, NCSe$^-$ and N(CN)$_2$$^-$, while with NCO$^-$, only the five-coordinate complex [Co(12-TMC)(NCO)][B(C$_6$H$_5$)$_4$] (**4**) was formed (Scheme 1). We have tried to use excess NCO$^-$ salt to prepare the six-coordinate analogue, but only five-coordinate complex **4** was formed. Such unusual behavior was rarely observed. Khan et al. observed the different coordination modes between the dinuclear copper(II) complexes with NCO$^-$ and NCS$^-$.[27]

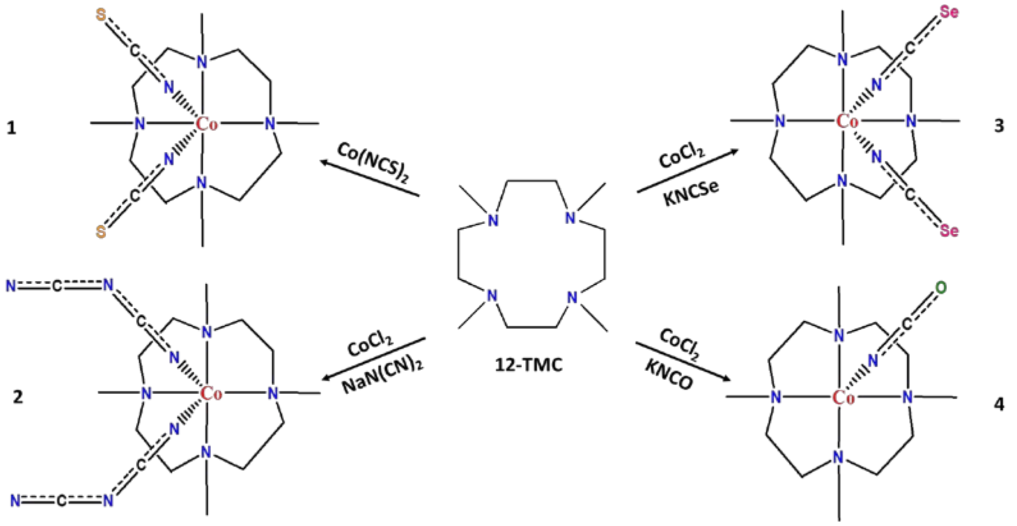

Scheme 1. Synthetic routes to complexes **1**-**4**.

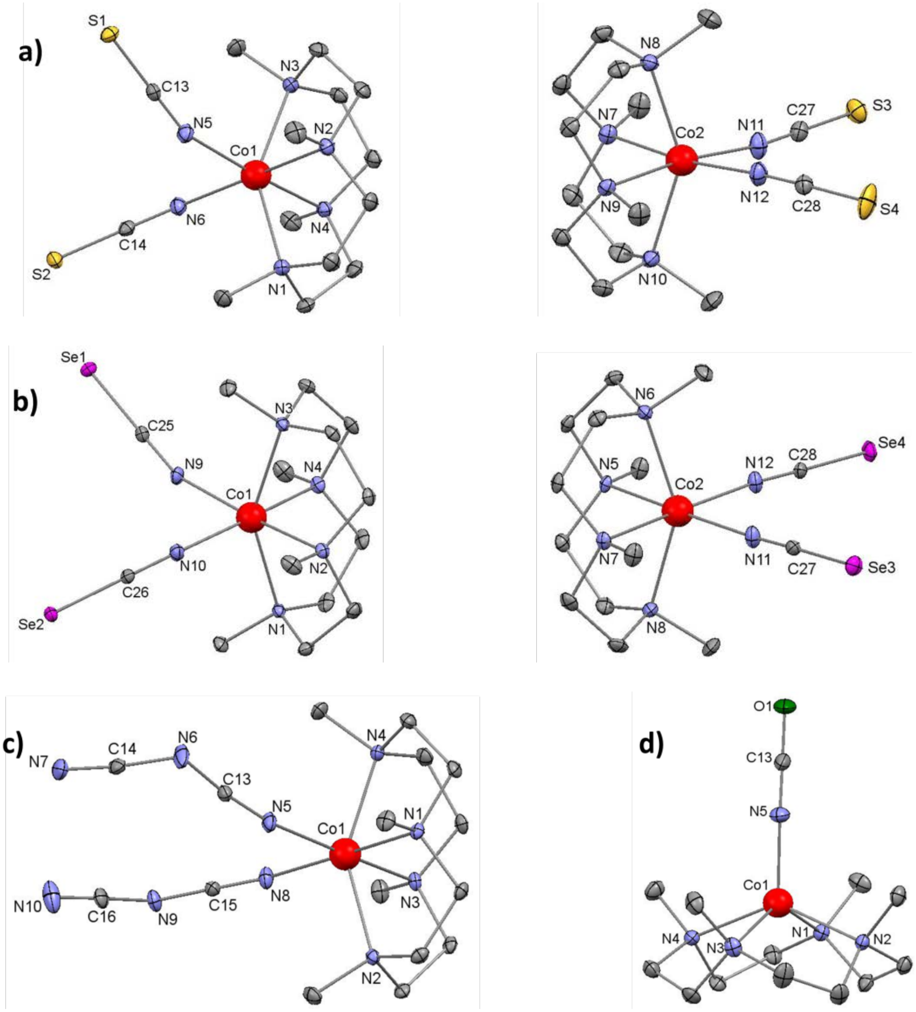

Fig. 1 (a) The octahedral Co^{II} ions of two different molecules in the asymmetric unit of **1** (30% probability); (b) The two octahedral Co^{II} ions of two different molecules in the asymmetric unit of **2** (30% probability); (c) The octahedral Co^{II} ion in **3** (30% probability); (d) The square pyramidal Co^{II} ion in **4** (30% probability). Red, blue, and gray spheres represent Co, N, and C atoms, and yellow, purple and green ones represent S, Se and O, respectively. All H atoms and solvent water molecules were omitted for clarity.

Structural descriptions

Complexes **1**, **2** and **3** crystallize in the monoclinic space group *P* $2_1/n$ (Table S1). Selected bond lengths and bond angles are afforded in Table S2. In contrast with only one unique molecule in **3** and **4**, the asymmetric unit of complexes **1** and **2** consist of two crystallographically distinct molecules. The distinct molecules are labelled as **1a**, **1b** and **2a**, **2b** (Fig. 1), whose structural parameters vary slightly. The central Co^{II} ions of these six-coordinate complexes are coordinated by six N atoms and adopt the distorted octahedral geometry. The two N atoms of pseudohalogen ions (NCS^{-}, **1**; NCSe^{-}, **2**; NCNCN^{-}, **3**) in *cis* positions and two tertiary amine N atoms from the neutral tetradentate macrocyclic ligand 12TMC define the equatorial plane while the remaining two tertiary nitrogen atoms occupy the axial positions (Fig. 1a, 1b and 1c). In the equatorial positions, Co−N$_{\text{pseudohalide}}$ bonds in a range of 2.065(3)−2.1058(14) Å are shorter than the bond distances between Co^{II} ion and the two N atoms of 12TMC ligand (2.252(3)−2.2826(13) Å), which are in turn larger than the Co−N$_{12\text{TMC}}$ bond distances in the axial positions (2.161(3)−2.195(3) Å). The equatorial N−Co−N bond angle involving the two *cis*- pseudohalide groups (83.38(6)−86.33(12)°) are smaller than that involving the two *cis*-N atoms of 12TMC ligand (100.99(9)−102.29(5)°). All of the angles in the equatorial plane deviate from the angle for an ideal octahedron with 90°. These angle distortions give a trapezoid in the equatorial plane. Furthermore, the axial bond angles between Co^{II} ion and the N atoms of 12TMC ligand are more bent with a range of 146.76(10)−147.80(10)° compared with the bond angle for an ideal octahedron (180°). Such tilting of two axial ligands combining with the distortion of the equatorial base leads to a skew-trapezoidal bipyramid configuration for **1**-**3**.[28]

In addition, a geometrical analysis was performed with the SHAPE program,[29] which is used to evaluate the degree of deviation from the ideal symmetry. The continuous shape measures (*CShMs*) of the Co^{II} centers show that the distortion value is 3.277, 3.230 and 2.967 for **1**, **2** and **3**, respectively, indicating that their molecular geometries are distorted octahedral (Table S3, ESI†). Besides, there is no intermolecular interaction, such as hydrogen bonds, except for *van der Waals'* forces in the crystal lattice. The average shortest intermolecular Co---Co distances are 7.905 Å for **1**, 7.987 Å for **2** and 8.055 Å for **3**, respectively.

It is noted that the similar coordination geometry of two molecules in complexes **1** and **2**, but the most obvious difference is the bond angles between Co^{II} ion and the pseudohalogen ions. For **1**, the two Co−N$_{\text{NCS}}$−C$_{\text{NCS}}$ bond angles are more bent with 149.3(3)° and 155.5(3)° in **1a** than those in **1b**, which are identical with 173.4(4)°. The corresponding Co−N−C bond angles are 153.2°and 155.4° in **2a**, 175.3°and 175.1° in **2b** and 163.20(15)° and 160.01(14)° in **3**. In addition, the two sets of N(CN)$_2^-$ of complex **3** bent in the opposite direction, wherein the C-N-C bond angles are 119.12° and 123.64°, respectively.

Complex **4** crystallizes in the monoclinic space group *P* $2_1/c$. It is five-coordinate with the Co(II) center residing in the distorted square pyramidal configuration, consisting of four N atoms from the 12-TMC ligand in the equatorial basal plane and one N atom from the NCO$^-$ group in the apical position (Fig. 1d). The Co(II) center lies out of the basal plane by 0.802 Å. The average Co−N$_{\text{equatorial}}$ bond distance is 2.161 Å, which is longer than the bond distances of Co−N$_{\text{NCO}}$ with 1.9399(17) Å. The greater basal angles of N-Co-N are almost equal with 136.0(2)° and 136.71(13)°, which is comparable to the structure expected for a perfectly square pyramidal complex with C_{4v} geometry. The shortest intermolecular Co---Co distance is 7.094 Å in **4**. Moreover, the continuous shape measures (*CShMs*) of the Co^{II} center were calculated by the SHAPE software.[29] The distortion value is 0.442 (Table S3, ESI†), which is close to zero for an ideal square pyramidal geometry.

Static magnetic properties and HF-EPR spectra

Direct-current (dc) magnetic susceptibilities were measured on polycrystalline samples of **1**-**4** under a dc field of 0.1 T in the 2−300 K temperature range. The obtained temperature dependence of $\chi_M T$ products are shown in Fig. 2 and S5-S7†. The room temperature $\chi_M T$ values are 2.66, 2.65, 2.61 and 3.01 cm^3 K mol^{-1} for **1-4**, respectively, which are higher than the theoretical spin-only value of 1.875 cm^3 K mol^{-1} for the mononuclear high-spin Co(II) center (S = 3/2, g = 2.0). They are in the reported range of 2.1−3.4 cm^3 K mol^{-1} for anisotropic high-spin Co(II) center,[30] which are ascribed to the significant orbital contribution. Upon cooling from room temperature, the $\chi_M T$ product remains constant until 80-90 K for **1**-**4**, and then slightly decreases to 1.68, 1.66, 1.65 and 1.97 cm^3 K mol^{-1}, respectively, at 2 K. The downturn of $\chi_M T$ value at low temperature is due to the inherent magnetic anisotropy of the Co^{II} ion rather than the intermolecular antiferromagnetic interactions between the metal ions considering the large intermolecular Co---Co separations.

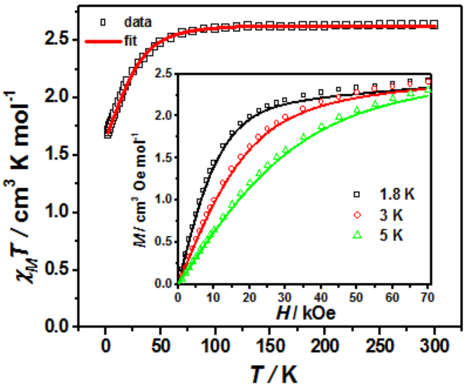

Fig. 2 Variable-temperature dc susceptibility data of **1** under applied dc field of 0.1 T Inset: field-dependent the magnetizations below 5 K. Solid lines are fits to the data with program *PHI*[32].

Furthermore, the field-dependent magnetisations were determined for **1**-**4** at applied magnetic fields ranging from 0 to 7 T at 1.8, 3.0 and 5.0 K, respectively (inset, Fig. 2, and S6-S7, ESI†). The magnetisation data affords the values of 2.42, 2.43, 2.47 and 2.44 $N_A\mu_B$ at 7 T and 1.8 K for **1**-**4**, respectively, which are far lower than the theoretical saturation value of 3 $N_A\mu_B$ for an isolated Co^{II} ion (g = 2, S = 3/2), indicating the magnetization of all four complexes does not achieve saturation at 7 T.

To analyse the magnitude and nature of the magnetic anisotropy, we employed the full Hamiltonian as given in eqn (1), which considers the strong orbital contribution to the magnetic moment for the Co(II) complexes where the unquenched orbital moment contributes strongly to the magnetic moment.

$$\hat{H} = \sigma\lambda\hat{L}\cdot\hat{S} + \sigma^2(B_2^0(3\hat{L}_z{}^2 - \hat{L}^2) + \frac{B_2^2}{2}(\hat{L}_+{}^2 + \hat{L}_-{}^2)) + \mu_B(\sigma\hat{L} + 2\hat{S})\cdot H \qquad (1)$$

where σ represents a combined orbital reduction parameter σ = −*A*·*κ*. The *A* parameter is required when using the T≡P equivalence for orbital triplet terms and takes the value of 1.0 when representing a T_2 term and 3/2 when representing a T_1 term. The *κ* parameter considers the reduction of the orbital momentum caused by the delocalization of the unpaired electrons. λ, B_2^0 and B_2^2 represent the spin-orbit coupling constant and crystal field parameters (CFPs)[31]. The fit to the dc magnetic susceptibilities of six-coordinate complexes **1**-**3** using *PHI*[32] program gives the reasonable parameters, which were listed in Table 1. The fitting curves match well with the experimental data in the range of whole temperature (Fig. S5, ESI†). From the fitting results of the magnetic susceptibilities above, it can be concluded that the parameters B_2^0 are positive, representing the easy-plane magnetic anisotropies, which are consistent with the following HFEPR data.

When the B_2^0 parameter is positive and relatively large, $^4A_{2g}$ can be considered as the ground term, which is well-separated from the excited term ^4E_g. Then, the energy gap between the two Kramers doublets of M_S = ±1/2 and M_S = ±3/2 splitting from the $^4A_{2g}$ term can be associated with an axial ZFS.[15a,15b] In this case, the magnetic properties may be interpreted with the spin Hamiltonian as shown in eqn. (2):

$$H = D(\hat{S}_z{}^2 - S(S+1)/3) + E(\hat{S}_x{}^2 - \hat{S}_y{}^2) + \mu_B g\hat{S}\cdot H \qquad (2)$$

where *D*, *E*, *S*, *H*, and μ_B represent the axial and rhombic ZFS parameters, the spin operator, magnetic field vectors, and the Bohr magneton, respectively. To estimate the zero-field splitting parameters *D* and *E* of the Co(II) centers in **1**-**3**, the experimental susceptibility and magnetization data were fit simultaneously using the program *PHI*.[32] The best-fit values of the parameters were showed in Table 1 for **1**-**3**. As we can see, the signs of ZFS parameters *D* are determined to be positive with the values of 32.10, 33.49, and 25.95 for **1**-**3**, respectively. These values show significant easy-plane anisotropies of the Co(II) centre in **1**-**3**.

For the five-coordinate complex **4** with the square-pyramid configuration, the orbital moment could contribute greatly to the magnetic properties.[14d,14e] The magnetic susceptibility data of **4** was also modelled with the general Hamiltanian as shown in eqn (1) by the program *PHI*[32]. It was found that no unique set of fitting parameters were obtained. To avoid the overparameterisation, we fix the rhombic crystal parameter B_2^2 as zero and treat magnetic data with three parameters *σ*, λ, and B_2^0. The fitting parameters are listed in Table 2. The negative value of B_2^0 shows the easy-axis magnetic anisotropy of **4**, which is in agreement with the HFEPR spectra.

To confirm the nature of the magnetic anisotropies in **1**-**4**, high-field and -frequency electron paramagnetic resonance (HFEPR) spectra[33] were recorded for the powder samples of **1**-**4** at different frequencies (Fig. 3 and S8-S11, ESI†).

Table 1. The fitting parameters obtained experimentally for complexes **1**-**4**.

	1	**2**	**3**	**4**
fittings of the dc magnetic data with eqn (1) by *PHI*.[32]				
Orbital reduction factor *σ*	-1.17(0)	-1.16(0)	-1.18(0)	-1.35(7)
λ, cm^{-1}	-82.66(8)	-88.72(1)	-73.83(4)	-88.17(4)
B_2^0, cm^{-1}	98.85(8)	102.23(5)	95.61(6)	-89.82(2)
B_2^2, cm^{-1}	96.94(9)	89.91(0)	85.94(6)	/
fittings of the dc magnetic data with eqn (2) by *PHI*.[32]				
D, cm^{-1}	32.10(0)	33.49(4)	25.95(9)	/
E, cm^{-1}	0.32(4)	0.16(9)	0.12(3)	/
$g_{x,y}$	2.46(2)	2.44(1)	2.43(4)	/
g_z	2.13(7)	2.20(9)	2.16(5)	/
Theoretical calculations of magnetic anisotropy				
D, cm^{-1}	26.6/24.5	27.4/25.9	22.5	/
E, cm^{-1}	8.8/8.1	8.9/-5.2	7.2	/
g_x	2.30/2.27	2.28/2.31	2.27	
g_y	2.55/2.52	2.54/2.50	2.48	/
g_z	2.14/2.12	2.11/2.11	2.12	/

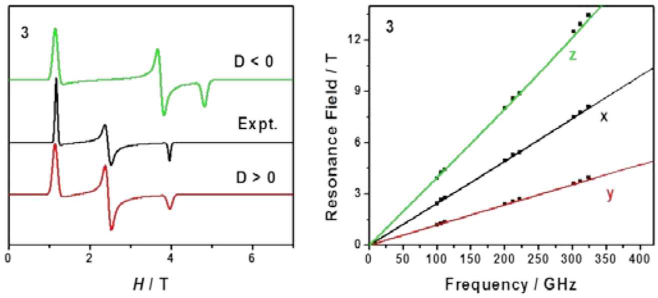

Fig. 3 Left: The experimental and simulation spectra for complex **3** under 100 GHz in derivative mode at 4.2 K. Right: Frequency dependence of the high-frequency EPR peak positions deduced from studies of powder samples of **3** at 4.2 K. The squares are the experimental points while green, blue, and red curves are generated by fitting using program *SPIN*[34] with the magnetic field parallel to the x, y, and z axes of the ZFS tensor, respectively.

For complex **3**, the spectrum at the frequency of 100 GHz at 4.2 K shows three features. Due to the large positive *D* value, only the Kramers doublet would be populated at low temperature and the observed resonances are attributed to the intra-Kramers transitions within the lowest doublet $M_S = \pm 1/2$ with $\Delta M_S = \pm 1$. The HFEPR spectrum can be easily interpreted as arising from an effective spin doublet (S_{eff} = 1/2) with strongly anisotropic g_{eff} factor.[15a,f,34] The effective *g* values [5.90, 3.89, 1.81] agree with a positive sign of *D* parameter for a spin 3/2 system.[15a,f,34]

A 2D resonating field versus frequency map was derived from the observed features and fit by the spin-Hamiltanian as shown in eqn (2)[35] (Fig. 3). Since the rhombicity factor (*E*/*D*), g_x and g_y values are intercorrelated, we cannot determine their accurate values. Using the magnitude of *D* obtained by fitting of the dc magnetic data (25.95 cm^{-1}), the simulations were done assuming an axial *g*-tensor ($g_x = g_y$), yielding the best parameter $g_x = g_y = 2.42$, $g_z = 2.18$ and *E* = + 6.5 cm^{-1}. In addition, by comparing the simulated spectrum with experimental one in Figure 3, the sign of *D* value was confirmed to be positive rather than negative. The average *g* value obtained is 2.34, which agrees well with 2.34 derived from the magnetic data. The value of *E*/*D* (0.25) is larger than that obtained from dc magnetic data. It is noted that the fitting of dc magnetic data is not sensitive to the *E* value. But the value of *E/D* is quite precisely defined by EPR data. Therefore the degree of axiality is much better estimated via EPR rather than via magnetic measurements.

For complexes **1**-**2**, there are two sets of three EPR features observed, which are in accordance with the two crystallographically different molecules in the crystal lattices (Fig. S8-S9, ESI†). The patterns of effective *g* values (g_x, $g_y > g_z$) are also in agreement with the large and positive *D* values.[15a,34]

The HFEPR spectra for the powdered sample of **4** at 4.2 K and 112 GHz (Fig. S10, ESI†) shows only a single parallel-type transition occurring at an effective *g* value of g^{eff} =7.01(4). There is only one strong signal observed at $g^{eff} \approx 7$, confirming the easy-axis type anisotropy for the Co(II) center.[13d,36] These observations are in agreement with the results obtained by fitting the magnetic data of **4**.

Theoretical studies of magnetic anistropy in 1-4

In order to get further insight into the nature of the magnetic anisotropies of **1**-**4**, theoretical studies were performed on **1**-**4** by the complete active space second-order multiconfigurational perturbation theory (CASPT2) considering the effect of the dynamic electron correlation based on complete-active-space self-consistent field (CASSCF) method with MOLCAS 8.2 program package. Calculation details are given in ESI†.

The energies of the spin-free states and spin-orbit states were calculated, which are listed in Tables S3-S4†. The first excited spin-free state is in the range of 1440.1-1687.2 cm^{-1} above the ground one for **1**-**3**, which means that the lowest quartet term is well isolated from the excited ones for **1**-**3**. These energy differences between the lowest two spin-free states are much larger than those between the lowest two spin-orbit states. Furthermore, the spin-orbit ground states are mainly composed from the ground one. The orbital nondegeneracy of the ground term allow us to use spin Hamiltanian as shown in eqn (2) with the ZFS parameters *D* and *E* to model their magnetic anisotropies. The calculated *D, E* (cm^{-1}) and *g* tensor (*x, y, z*) of **1**–**3** are listed in Table S5†. The calculated *D* values are +26.6, +24.5, +27.4, +25.9 and +22.5 cm^{-1} for **1a**, **1b**, **2a**, **2b** and **3**, respectively, which are comparable to those derived from the magnetic data. The average calculated *g* values are 2.32, 2.31 and 2.30 for **1**, **2** and **3**, respectively, which are in consistent with those derived from the magnetic data (2.35, **1**; 2.36, **2**; 2.34, **3**).The calculated $\chi_M T$ versus *T* and *M* versus *H* plots of **1**–**3** are shown in Fig. S12-S13†. The calculated orientations of the local main magnetic axes on Co^{II} ion of **1**–**3** are shown in Fig. S14†.

For complex **4**, the energy gap (375.7 cm^{-1}) between the lowest two spin-free states is in agreement with the quasi-degeneracy related to the ^{4}E term in the idealized C_{4v} symmetry.[14d,14e] This energy gap is larger than that between the lowest two spin-orbit states (162.3 cm^{-1}). However, the spin-orbit ground state is composed from the lowest two spin-free states, not just from the ground one (Table S5, ESI†). These suggest that there is very strong first-order spin-orbital coupling in **4** and zero-field splitting parameters *D* and *E* cannot be used to depict its magnetic anisotropy. Therefore the traditional spin Hamiltanian cannot be used to model the magnetic data and HFEPR spectra.[14d,14e] The calculated *S* = 1/2 effective *g*-values of the ground state Kramers doublet of the Co^{II} centre of **4** are g_x = 0.541, g_y = 0.735, and g_z = 9.253 (Table S7, ESI†), demonstrating its easy-axis anisotropy. The magnetic susceptibilities of **4** were also calculated as shown in Fig. S12†, which are comparable to the experimental curves. Furthermore, the calculated orientations of the g_x, g_y, g_z (easy-axis) of the ground doublet on the Co^{II} ion was shown in Fig. S13†.

Dynamic magnetic properties

To investigate the relaxation dynamics of **1**–**4**, alternating-current (ac) susceptibility measurements were carried out in the temperature range of 1.8–6 K with an alternating field of 0.2 mT oscillating with 1–999 Hz under different dc fields (Fig. 4 and S14-S25, ESI†). Unfortunately, no out-of-phase (χ_M'') signals were detected under zero applied dc field. However, all complexes exhibit strong frequency-dependent ac susceptibilities under a small external dc field. The absence of out-of-phase (χ_M'') signals under zero applied field could be caused by the occurrence of strong quantum tunneling of magnetization (QTM), which has been observed in most Co(II)-based single ion magnets.[11-17]

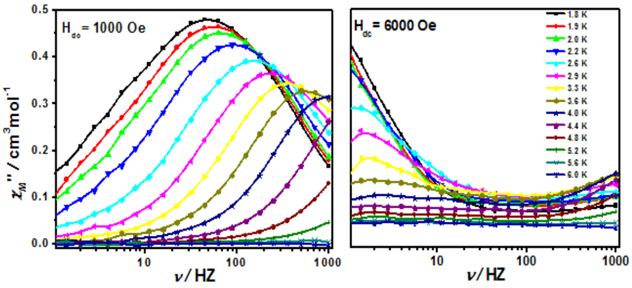

Fig. 4 Frequency dependence of the ac susceptibility from 1.8 to 6 K for **1** under 0.1 T (left) and 0.6 T (right). The solid lines are for eye guide.

For **1** and **2**, there is only one magnetic relaxation process under an external dc field from 0.02 to 0.1 T. However, two slow relaxations were observed in the χ_M'' vs ν plot with the increase of the external dc field until 0.6 T (Figure S14). Hence, 0.1 T and 0.6 T were chosen for **1** and 0.08 T and 0.6 T for **2** to perform further ac magnetic measurements in the temperature range of 1.8-6.0 K (Fig. 4 and S16-S22, ESI†). Under these two different external dc fields, only one slow magnetic relaxation was observed in the whole temperature range.

The plot of *ln(τ)* versus *H* at 1.8 K were extracted from the variable-frequency susceptibility data under different dc fields (Figure 5 and S15). Assuming the Raman and Orbach processes as a constant *k*(*T*) due to their weakly field-dependent, the dependence of *τ* on the field was analyzed by means of equation (3):[37]

$$\tau^{-1} = AH^4T + \frac{B_1}{1+B_2H^2} + k(T) \qquad (3)$$

where the first term represents direct process, the second term represents quantum tunneling of magnetization (QTM) and the last term represents the combination of Raman and Orbach processes. As shown in Fig. 5 and S15, the fitting curve accords well with the experimental data, giving the reasonable parameters, which were listed in Table 2.

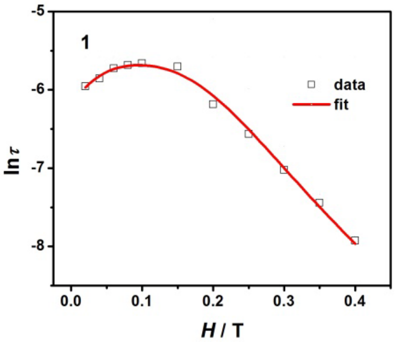

Fig. 5 Field dependence of the magnetization relaxation times for **1**. The red line represents the best fit by using eqn (3).

Table 2. The parameters fit by eqn (3) for complexes **1**-**4**.

	1	**2**	**3**	**4**
a, s^{-1} T^{-4} K^{-1}	56675.3(5)	20017.9(3)	485.4(6)	74076.7(6)
B_1, s^{-1}	164.7(1)	1035.3(3)	112.0(1)	85.4(7)
B_2, T^{-2}	844.5(1)	151.2(4)	1322.2(0)	598.8(1)
$k(T)$, s^{-1}	267.3(6)	33.6(8)	18.9(2)	116.7(9)

The plot of $ln(\tau)$ versus T^{-1} were extracted from the peak value of the variable-frequency susceptibility data under different temperatures. We have tried to model the relaxation rates employing the direct, QTM, Raman and Orbach relaxation processes by using eqn (4):

$$\tau^{-1} = AH^4T + \frac{B_1}{1+B_2H^2} + CT^n + \tau_0^{-1}\exp(-U_{eff}/kT) \qquad (4)$$

where the first, second, third and last term represents direct, QTM, Raman and Orbach process, respectively. It was found that no reasonable parameters could be obtained when including the Orbach process, the temperature dependence of the magnetization relaxation of **1** and **2** were fit by direct, QTM and Raman processes. By fixing these obtained coefficients of direct and QTM processes from the fitting of the plot of $ln(\tau)$ versus H at 1.8 K, the successful fit is in accord with the experimental data over the whole temperature range, yielding the following parameters: C = 38.24 s^{-1} K$^{-3.58}$, n = 3.58 for **1** and C = 1.76 s^{-1} K$^{-6.19}$, n = 6.19 for **2** (Fig. 6a and S23, ESI†). It can be seen that the optical acoustic Raman-like mechanism is predominated in the whole studied temperature range for **1** and the Raman process is dominated in high temperature range while the QTM process dominates in the low temperature range for **2**.

The Cole–Cole plots from the ac magnetic susceptibility data of **1** under 0.1 T and **2** under 0.08 T were also constructed (Fig. 5b and S25, ESI†) and fit by the generalized Debye model[38] to give the isothermal susceptibility (χ_T), adiabatic susceptibility (χ_S), τ, and α parameters. The α parameters are in a range of 0.10–0.41 for **1** and 0.08–0.33 for **2**, suggesting the relatively narrow distribution of the relaxation time (Table S8, ESI†).

Relaxation times under 0.6 T for **1-2** were extracted from the peak values of the temperature dependence of out-of-phase ac susceptibilities (χ_M'') in the high-frequency and –temperature region. It can be considered that the Orbach mechanism is the dominant process under 0.6 T. The $ln(\tau)$ vs T^{-1} plots were fit with Arrhenius' law $\tau = \tau^0 exp(U_{eff}/k_BT)$ (Fig. S24, ESI†). We can derive the effective energy barrier with the preexponential factor as U_{eff} = 23.23 cm^{-1} (τ_0 = 3.0 × 10^{-8} s) for **1**, U_{eff} = 25.53 cm^{-1} (τ_0 = 1.8 × 10^{-8} s) for **2**.

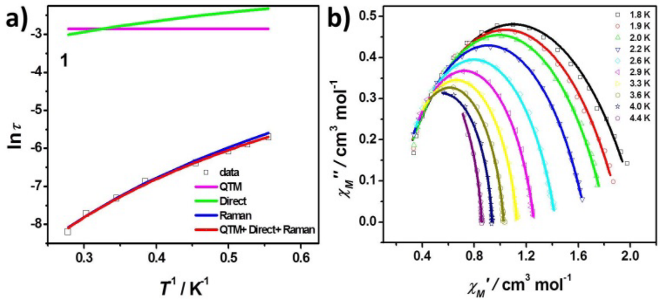

Fig. 6 (a) Relaxation time of the magnetization $ln(\tau)$ vs T^{-1} plots for **1**. (b) Cole-Cole plot obtained from the ac susceptibility data under different range of temperature for **1**. Solid lines represent the best fits to a generalized Debye model[38].

There is only one magnetic relaxation process under an external dc field in **3** and **4**. 0.2 T and 0.1 T fields were chosen to perform additional ac measurements, respectively (Fig. S26-S29, ESI†). Their plots of $ln(\tau)$ versus H at 1.8 K were similarly fit as **1** and **2**. The plots of $ln(\tau)$ versus T^{-1} of **3** and **4** extracted from the variable-frequency susceptibility data were fit using eqn (4). By fixing these obtained coefficients of direct and QTM processes from the fitting of the plot of $ln(\tau)$ versus H at 1.8 K, the fitting gave the following parameters of C = 1.54 s^{-1}K$^{-4.19}$, n = 4.19, τ_0 = 1.14 × 10^{-8} s, U_{eff} = 27.31 cm^{-1} for **3** and C = 6.57 s^{-1}K$^{-5.48}$, n = 5.48, τ_0 = 1.17 × 10^{-9} s, U_{eff} = 23.16 cm^{-1} for **4** (Fig. S30, ESI†). It shows that the QTM and direct process are not dominated over the whole studied temperature range and thus can be negligible. The Raman process is the dominated mechanism at the low temperature region while the Orbach mechanism dominates at high temperature range for both **3** and **4**.

The Cole–Cole plots (Fig. S31, ESI†) were also constructed for **3** and **4** by fitting of the χ_M'' versus χ_M' data by the generalized Debye model,[38] yielding the isothermal susceptibility (χ_T), adiabatic susceptibility (χ_S), τ, and α parameters, which are listed in Table S7†. The obtained α parameters are in the range of 0.08-0.35 and 0.09-0.17 for **3** and **4**, respectively. Compared with six-coordinate Co(II) complexes **1**, **2** and **3**, the five-coordinate Co(II) complexes of **4** signifies a narrower relaxation distribution.

In order to get further insight into the dynamics mechanisms for the magnetic relaxation of **1**-**4**, we have tried to prepare the diluted samples via co-preparation starting with a 1:9 stoichiometry of Co(II) and Zn(II) salts. However, there was no desired diluted sample obtained. Then we intended to synthesize the pure Zn(II) complexes at first and then prepare the diluted samples by cocrystallization of Co(II) complexes and its isostructrual Zn(II) analogue. However, the pure Zn(II) complexes obtained were all five-coordinate. Although we did not obtain the diluted samples for six-coordinated complexes of **1**, **2** and **3**, the diluted sample for five-coordinate complex **4** was synthesized successfully, which was confirmed by XRD (Fig. S32, ESI†) and ICP data.

Alternative current (ac) susceptibilities of the diluted sample **4'** were measured under different external dc fields at 1.8 K. As shown in Fig. S33†. The diluted complex **4'** exhibits no response of out-of phase magnetic susceptibility (χ_M'') under zero static field. Again, a non-zero χ_M'' response was observed under an applied external dc field. For comparison, an optimum dc field of 0.10 T was also chosen to further investigate the ac magnetic susceptibilities of complex **4'** (Fig. S34, ESI†). The plot of $ln(\tau)$ versus T^{-1} extracted from the variable-frequency susceptibility data was fit by the Raman and Orbach processes, giving the following parameters of $C = 1.5\ s^{-1}K^{-7.3}$, $n = 7.3$, $\tau_0 = 1.7 \times 10^{-10}$ s, $U_{eff} = 25.6\ cm^{-1}$ for **4'** (Fig. S35, ESI†). Similar with complex **4**, the Raman process is the dominated mechanism at the low temperature region while the Orbach mechanism dominates at high temperature range in **4'**. The relaxation time τ extracted from frequency-dependent data of complexes **4** and **4'** are largely similar in the whole temperature range (Fig. S36, ESI†). The Cole−Cole plots (Fig. S37, ESI†) were also constructed by fitting of the χ_M'' versus χ_M' data by the generalized Debye model,[38] yielding the α parameters in the range of 0.02-0.20 for **4'** (Table S9, ESI†). In summary, there is no significant change in the dynamics properties before and after dilution in the studied temperature range.

Conclusions

This report presents the synthesis and characterization of four field-induced SIMs based on Co^{II} ion supported by a macrocyclic ligand 12TMC, which are coordinated by the pseudohalogen ligands, namely, NCS^- (**1**), $NCSe^-$ (**2**), $N(CN)_2^-$ (**3**) and NCO^- (**4**). Different from six-coordinate complexes **1**, **2**, and **3**, complex **4** is five- coordinated with NCO^- occupying at the axial position. Through changing the pseudohalido ligands, distortions around the metal center were modulated to induce different magnetic anisotropy. It can be revealed that there are easy-plane anisotropy in all six-coordinate complexes by direct magnetic measurements and HFEPR spectroscopy and theoretical studies, while it is easy-axis anisotropy in five-coordinate complex. For six-coordinate complexes **1**-**3**, D values obtained by fitting with the dc magnetic susceptibilities decrease in the trend of D ($NCSe^-$) > D (NCS^-) > D ($N(CN)_2^-$), which are in accordance with the trend predicted by theoretical calculation. The detailed study of the dynamic susceptibilities revealed that **1** and **2** show two slow relaxation processes under an external dc field. Although various pseudohalide ligands result in distinct slow magnetic relaxation mechanisms, the Raman process plays an important role in all complexes. The present work shows that the magnetic anisotropy and the slow relaxation dynamics of Co(II) complexes can be fine-tuned by structural modification by the pseudohalides.

Conflicts of interest

There are no conflicts to declare.

Acknowledgements

We are grateful for the financial support from the Natural Science Grant of China (No. 21471078 to XTC and and 11774178 to YQZ) and the US National Science Foundation (CHE-1633870 to ZLX).

Notes and references

1 (a) M. N. Leuenberger and D. Loss, *Nature*, 2001, **410**, 789–793; (b) M. Affronte, *J. Mater. Chem.*, 2009, **19**, 1731–1737; (c) F. Troiani and M. Affronte, *Chem. Soc. Rev.*, 2011, **40**, 3119–3129.

2 (a) L. Bogani and W. Wernsdorfer, *Nat. Mater.*, 2008, **7**, 179–186; (b) M. Urdampilleta, S. Klyatskaya, J.-P. Cleuziou, M. Ruben and W. Wernsdorfer, *Nat. Mater.*, 2011, **10**, 502–506.

3 (a) W. Wernsdorfer, N. A. Alcalde, D. N. Hendrickson and G. Christou, *Nature*, 2002, **416**, 406; (b) S. Thiele, F. Balestro, R. Ballou, S. Klyatskaya, M. Ruben and W. Wernsdorfer, *Science*, 2014, **344**, 1135−1138.

4 (a) N. Ishikawa, M. Sugita, T. Ishikawa, S. Y. Koshihara and Y. Kaizu, *J. Am. Chem. Soc.*, 2003, **125**, 8694–8695; (b) J. D. Rinehart, M. Fang, W. J. Evans and J. R. Long, *Nat. Chem.*, 2011, **3**, 538–542; (c) D. N. Woodruff, R. E. P. Winpenny and R. A. Layfield, *Chem. Rev.*, 2013, **113**, 5110–5148; (d) H. L. C. Feltham and S. Brooker, *Coord. Chem. Rev.*, 2014, **276**, 1–33.

5 (*a*) G. A. Craig and M. Murrie, *Chem. Soc. Rev*. 2015, **44**, 2135-2147; (*b*) A. K. Bar, C. Pichon and J.-P. Sutter, *Coord. Chem. Rev.*, 2016, **308**, 346-380; (*c*) J. M. Frost, K. L. M. Harriman and M. Murugesu, *Chem. Sci.*, 2016, **7**, 2470-2491; (*d*) M. Feng and M.-L. Tong, *Chem. Eur. J.* 2018, **24**, 7574–7594.

6 Y.-F. Deng, T. Han, Z. Wang, Z. W. Ouyang, B. Yin, Z. P. Zheng, J. Krzystek and Y.-Z. Zheng, *Chem. Commun,*. 2015, **51**, 17688−17691.

7 (a) L. Chen, J. Wang, Y.-Z. Liu, Y. Song, X.-T. Chen, Y.-Q. Zhang and Z.-L. Xue, *Eur. J. Inorg. Chem.*, 2015, **2**, 271–278; (b) J. Vallejo, A. Pascual-Alvarez, J. Cano, I. Castro, M. Julve, F. Lloret, J. Krzystek, G. De Munno, D. Armentano, W. Wernsdorfer, R. Ruiz-Garcia and E. Pardo, *Angew. Chem. Int. Ed.*, 2013, **52**, 14075−14079; (c) M. Ding, G. E. Cutsail III, D. Aravena, M. Amoza, M. Rouzières, P. Dechambenoit, Y. Losovyj, M. Pink, E. Ruiz, R. Clèrac and J. M. Smith, *Chem. Sci.*, 2016, **7**, 6132-6140.

8 (a) D. E. Freedman, W. H. Harman, T. D. Harris, G. J. Long, C. J. Chang and J. R. Long, *J. Am. Chem. Soc.*, 2010, **132**, 1224–1225;(b) J. M. Zadrozny, D. J. Xiao, M. Atanasov, G. J. Long, F. Grandjean, F. Neese and J. R. Long, *Nat. Chem.,* 2013, **5,** **5**77−581; (c) P. P. Samuel, K. C. Mondal, N. Amin Sk, H. W. Roesky, E. Ca**rl**, R. Neufeld, D. Stalke, S. Demeshko, F. Meyer, L. Un**g**ur, L. F. Chibotaru, J. Christian, V. Ramachandran, J. van Tol and N. S. Dala**l,** *J. Am. Chem. Soc.*, 2014, **136**, 11964−11971.

9 (a) R. C. Poulten, M. J. Page, A. G. Algarra, J. J. Le Roy, I. López, E. Carter, A. Llobet, S. A. Macgregor, M. F. Mahon, D. M. Murphy, M. Murugesu and M. K. Whittlesey, *J. Am. Chem. Soc.*, 2013, **135**, 13640−13643; (b) K. E. R. Marriott, L. Bhaskaran, C. Wilson, M. Medarde, S. T. Ochsenbein, S. Hill and M. Murrie, *Chem Sci.*, 2015, **6**, 6823-6828.

10 R. Boča, C. Rajnák, J. Titič and D. Valigura, *Inorg. Chem.*, 2017, **56**, 1478-1482.

11 P. C. Bunting**,** M. Atanasov, E. Damgaard-MØller, M. Perfetti, I. Crassee, M. Orlita, J. Overgaard, J. V. Slageren, F. Neese and J. R. Long, *Science*, 2018, **362**, eaat7319(1-9).

12 (a) A. Eichhöfer, Y. Lan, V. Mereacre, T. Bodenstein and F. Weigend, *Inorg. Chem.*, 2014, **53**, 1962−1974; (b) F. Deng, T. Han, B. Yin and Y.-Z. Zheng, *Inorg. Chem. Front.*, 2017, 4, 1141–1148.

13 (a) J. M. Zadrozny and J. R. Long, *J. Am. Chem. Soc.*, 2011, **133**, 20732–20734; (b) J. M. Zadrozny, J. Liu, N. A. Piro, C. J. Chang, S. Hill and J. R. Long, *Chem. Commun.*, 2012, **48**,

3927–3929; (c) .Y. Rechkemmer, F. D. Breitgoff, M. van der Meer, M. Atanasov, M. Hakl, M. Orlita, P. Neugebauer, F. Neese, B. Sarkar and J. van Slageren, *Nat. Commun.*, 2016, **7**, 10467; (d) P. Cucos, F. Tuna, L. Sorace, I. Matei, C. Maxim, S. Shova, R. Gheorghe, A. Caneschi, M. Hillebrand and M. Andruh, *Inorg. Chem.*, 2014, **53**, 7738−7747; (e) S. Vaidya, S. K. Singh, P. Shukla, K. Ansari, G. Rajaraman and M. Shanmugam, *Chem. Eur. J.*; 2017, **23**, 954 –9559; (f) J.-J. Liu, Y.-S. Meng, I. Hlavička, M. Orlita, S.-D. Jiang, B.-W. Wang and S. Gao, *Dalton Trans.*, 2017, **46**, 7408–7411.

14 (a) T. Jurca, A. Farghal, P.-H. Lin, I. Korobkov, M. Murugesu and D. S. Richeson, *J. Am. Chem. Soc.*, 2011, **133**, 15814-15817; (b) T. J. Woods, M. F. Ballesteros-Rivas, S.Gómez-Coca, E. Ruiz and K. R. Dunbar, *J. Am. Chem. Soc.*, 2016, **138**, 16407−16416; (c) A. K. Mondal, T. Goswami, A. Misra and S. Konar, *Inorg. Chem.*, 2017, **56**, 6870−6878; (d) C. Rajnák, F. Varga, J. Titiš, J. Moncoľ and R. Boča, *Eur. J. Inorg. Chem.* 2017, 1915–1922; (e) A. Świtlicka, B. Machura, M. Penkala, A. Bieńko, D. C. Bieńko, J. Titiš, C. Rajnák and R. Boča, *Inorg. Chem.*, 2018, **57**, 12740−12755.

15 (a) J. Vallejo, I. Castro, R. Ruiz-García, J. Cano, M. Julve, F. Lloret, G. De Munno, W. Wernsdorfer and E. Pardo, *J. Am. Chem. Soc.*, 2012, **134**, 15704−15707; (b) A. V. Palii, D. V. Korchagin, E. A. Yureva, A. V. Akimov, E. Y. Misochko, G. V. Shilov, A. D. Talantsev, R. B. Morgunow, S. M. Aldoshin and B. S. Tsukerblat, *Inorg. Chem.*, 2016, **55**, 9696−9706; (c) M. A. Palacios, J. Nehrkorn, E. A. Suturina, E. Ruiz, S. Gjmez-Coca, K. Holldack, A. Schnegg, J. Krzystek, J. M. Moreno, and E. Colacio, *Chem. Eur. J.,* 2017, **23**, 11649–11661; (d) L. Váhovská, S. Vitushkina,. I. Potočňák, Z. Trávníček and R. Herchel, *Dalton Trans.*, 2018, **47**, 1498–1512. (e) S. Gómez-Coca, A. Urtizberea, E. Cremades, P. J. Alonso, A. Camón, E. Ruiz and F. Luis, *Nat. Commun*. 2014, **5**, 4300 (1-8); (f) L. Rigamonti, N. Bridonneau, G. Poneti, L. Tesi, L. Sorace, D. Pinkowicz, J. Jover, E. Ruiz, R. Sessoli and A. Cornia, *Chem. Eur. J.,* 2018, **24**, 8857–8868.

16 (a) L. Chen, S.-Y. Chen, Y.-C. Sun, Y.-M. Guo, L. Yu, X.-T. Chen, Z.-X. Wang, Z. W. Ouyang, Y. Song and Z.-L. Xue, *Daton. Trans.*, 2015, **44**, 11482-11490; (b) X.-C. Huang, C. Zhou, D. Shao and X.-Y. Wang, *Inorg. Chem*., 2014, **53**, 12671-12673.

17 L. Chen, J. Wang, J.-M. Wei, W. Wernsdorfer, X.-T. Chen, Y.-Q. Zhang, Y. Song and Z.-L. Xue, *J. Am. Chem. Soc.*, 2014, **136**, 12213−12216.

18 (a) J. M. Zadrozny, J. Telser and J. R. Long, *Polyhedron*, 2013, **64**, 209−217; (b) F. Shao, B. Cahier, E. Riviere, R. Guillot, N. Guihery, V. E. Campbell and T. Mallah, *Inorg. Chem.*, 2017, **56**, 1104−1111; (c) M. R. Saber and K. R. Dunbar, *Chem. Commun.,* 2014, **50**, 12266−12269; (d) X.-N. Yao, M.-W. Yang, J. Xiong, J.-J. Liu, C. Gao, Y.-S. Meng, S.-D. Jiang, B.-W. Wang and S. Gao, *Inorg. Chem. Front.*, 2017, **4**, 701–705.

19 H.-H. Cui, J. Wang, X.-T. Chen and Z.-L. Xue, *Chem. Commun.*, 2017, **53**, 9304-9307.

20 J. Cho, R. Sarangi, H. Y. Kang, J. Y. Lee, M. Kubo, T. Ogura, E. I. Solomon and W. Nam, *J. Am. Chem. Soc.*, 2010, **132**, 16977-16986.

21 (a) B. Cage, A. Hassan, L. Pardi, J. Krzystek, L. C. Brunel and N. S. Dalal, *J. Magn. Reson.*, 1997, **124**, 495-498; (b) A. Hassan, L. Pardi, J. Krzystek, A. Sienkiewicz, P. Goy, M. Rohrer and L. C. Brunel, *J. Magn. Reson.*, 2000, **142**, 300-312.

22 *SMART & SAINT Software Reference Manuals, version 6.45*; Bruker Analytical X-ray Systems, Inc.: Madison, WI, 2003.

23 SAINT, *Program for Data Extraction and Reduction*, Siemens Analytical X-ray Instruments, Madison, WI, 1994–1996.

24 G. M. Sheldrick, *SADABS: Software for Empirical Absorption Correction, version 2.05*; University of Göttingen: Göttingen, Germany, 2002.

25 G. M. Sheldrick, *SHELXL-2014: Program for Crystal Structure Refinement*; University of Göttingen: Göttingen, Germany, 2014.

26 G. A. Bain and J. F. Berry, *J. Chem. Educ.*, 2008, **85**, 532-536.

27 S. Khan, S. Sproules, L. S. Natrajan, K. Harms and S. Chattopadhyay, *New J. Chem.,* 2018, **42**, 1634–1641.

28 S. Alvarez, D. Avnir, M. Llunell and M. Pinsky, *New J. Chem.*, 2002, **26**, 996–1009.

29 (*a*) M. Llunell, D. Casanova, J. Cirera, P. Alemany and S. Alvarez, *Shape Program*, Version 2.1, 2013; (*b*) S. Alvarez, P. Alemany, D. Casanova, J. Cirera, M. Llunell and D. Avnir, *Coord. Chem. Rev.*, 2005, **249**, 1693-1708.

30 F. E. Mabbs and D. J. Machin, *Magnetism and Transition Metal Complexes*; Dover Publications: Mineola, NY, 2008.

31 (a) F. Lloret, M. Julve, J. Cano, R. Ruiz-García and E. Pardo, *Inorg. Chim. Acta*, 2008, **361**, 3432-3445; (b) J. Titiš and R. Boča, *Inorg. Chem.*, 2011, **50**, 11838-11845.

32 N. F. Chilton, R. P. Anderson, L. D. Turner, A. Soncini and K. S. Murray, *J. Comput. Chem.*, 2013, **34**, 1164−1175.

33 (a) J. Krzystek, O. Ozarowski and J. Telser, *Coord. Chem. Rev.*, 2006, **250**, 2308−2324; (b) J. Krzystek, S. A. Zvyagin, O. Ozarowski, S. Trofimenko and J. Telser, *J. Magn. Reson.*, 2006, **178**, 174−183.

34 (a) L. Banci, A. Bencibi, C. Benelli, D. Gatteschi and C. Zanchini, *Struct. Bonding*, 1982, **52**, 37-86; (b) J. R. Pilbrow, *J. Magn. Reson.*, 1978, **31**, 479-490.

35 Simulations were performed using SPIN developed by Andrew Ozarowski at the National High Magnetic Field Laboratory, USA.

36 W. D. Horrocks and D. A. Burlone, *Inorg. Chim. Acta,* 1979, **35**, 165-175.

37 (*a*) A. Abragam and B. Bleaney, *Electron paramagnetic resonance of transition ions*, Dover, New York, 1986; (*b*) A. Fort, A. Rettori, J. Villain, D. Gatteschi and R. Sessoli, *Phys. Rev. Lett.*, 1998, **80**, 612–615; (c) E. Lucaccini, L. Sorace, M. Perfetti, J.-P. Costes and R. Sessoli, *Chem. Commun.*, 2014, **50**, 1648–1651.

38 (a) K. S. Cole and R. H. Cole, *J. Chem. Phys.*, 1941, **9**, 341−351; (*b*) Y.-N. Guo, G.-F. Xu, Y. Guo and J. Tang, *Dalton Trans.*, 2011, **40**, 9953-9963.